

# H $\alpha$ Kinematics of the Largest DSFGs at $z \sim 1.5$

Patrick Drew<sup>1</sup>, Caitlin Casey<sup>1</sup>, Chao-Ling Hung<sup>1</sup>, Asantha Cooray<sup>2</sup>, Dave Sanders<sup>3</sup>, Hai Fu<sup>4</sup>

<sup>1</sup> University of Texas at Austin, <sup>2</sup> University of California Irvine, <sup>3</sup> University of Hawaii, <sup>4</sup> University of Iowa

## Abstract

We present a rest-frame optical kinematic analysis of five DSFGs at  $z \sim 1.5$  using long slit spectroscopy obtained with the MOSFIRE spectrograph on Keck I. Our sample was selected from Casey+13/Casey+17 samples based on their large angular sizes and interesting kinematic profiles. From our high signal-to-noise spectra we simultaneously fit H $\alpha$ , [NII]  $\lambda$ 6548, and [NII]  $\lambda$ 6583, where extant, at successive points along each slit to generate position-velocity and position-dispersion diagrams. We analyze these diagrams in context with Hubble ACS imaging for evidence of merging activity and find that our merging systems lie below the main sequence of galaxies at  $z \sim 1.5$ , suggesting sSFR may not be a useful discriminator of star formation mechanisms at high  $z$ . Using MAGPHYS we fit ancillary photometry from the COSMOS collaboration to estimate star formation rates, infrared luminosities, and stellar masses. We estimate dynamical masses for two galaxies which display no firm evidence of merging activity. The average half light radius of our sample, 10 kpc, is  $\sim 3$  times larger than the typical size of DSFGs.

Source	450.25	450.27	850.04	850.60	850.95
$Z_{\text{spec}}$	1.516	1.535	1.436	1.457	1.556
SFR [ $M_{\odot} \text{ yr}^{-1}$ ]	$136^{+66}_{-47}$	$382 \pm 47$	$111^{+66}_{-38}$	$211 \pm 38$	$283^{+113}_{-85}$
$L_{\text{IR}}$ [ $L_{\odot}$ ]	$(1.5^{+0.7}_{-0.5}) \times 10^{12}$	$(4.1 \pm 0.5) \times 10^{12}$	$(1.2^{+0.7}_{-0.4}) \times 10^{12}$	$(2.2 \pm 0.4) \times 10^{12}$	$(3.0^{+1.2}_{-0.9}) \times 10^{12}$
$M_{\star}$ [ $M_{\odot}$ ]	$(3.4 \pm 0.5) \times 10^{11}$	$(3.0 \pm 0.4) \times 10^{11}$	$(3.0 \pm 1.0) \times 10^{10}$	$(2.1 \pm 0.2) \times 10^{11}$	$(3.8 \pm 3.0) \times 10^{10}$
$M_{\text{dyn}}$ [ $M_{\odot}$ ]	—	—	$(4.6 \pm 1.0) \times 10^{10}$	—	$(1.7 \pm 0.8) \times 10^{11}$
$r_{1/2}$ [kpc]	$15.2 \pm 0.7$	$5.6 \pm 1.6$	$9.5 \pm 0.1$	$7.6 \pm 0.1$	$12.4 \pm 0.2$
$\sigma_{\text{avg}}$ [ $\text{km s}^{-1}$ ]	$87 \pm 23$	$148 \pm 57$	$107 \pm 13$	$88 \pm 42$	$71 \pm 56$

$Z_{\text{spec}}$  is calculated from the average velocity of H $\alpha$  in the galaxy. SFR,  $L_{\text{IR}}$ , and  $M_{\star}$  are estimated using MAGPHYS<sup>1,2</sup>. We only estimate  $M_{\text{dyn}}$  for galaxies that are unlikely to be late stage mergers.  $r_{1/2}$  is estimated by fitting UltraVISTA H-band data with GALFIT<sup>3,4</sup>. The average half light radius is  $10 \pm 3$  kpc,  $\sim 3$  times larger than the typical H-band size of DSFGs in the Chapman+05<sup>5</sup> sample.  $\sigma_{\text{avg}}$  is calculated from the measured dispersion of H $\alpha$  and [NII]. The errors are the standard deviation.

## Spectra

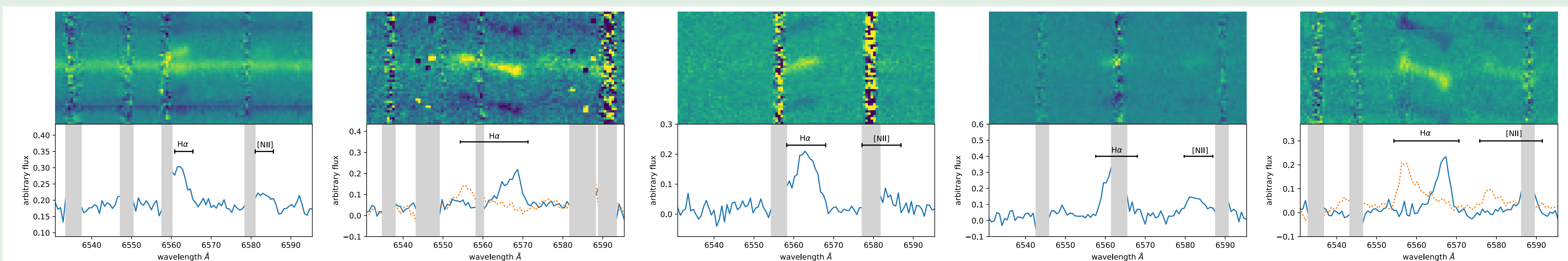
DSFG 450.25

DSFG 450.27

DSFG 850.04

DSFG 850.60

DSFG 850.95



**Top:** 2D MOSFIRE spectra. The vertical axis is spatial, and the horizontal axis is wavelength. The spectra are centered on the rest frame wavelength of the average velocity of H $\alpha$ . **Bottom:** Example 1D slices of 2D spectra. Telluric lines are plotted in grey. In galaxies where there is a wide range of velocities we plot an example slice from each extreme (orange dotted curve). The overall range of velocities associated with H $\alpha$  and [NII] in 2D is indicated by the horizontal black bars.

## PV Diagrams

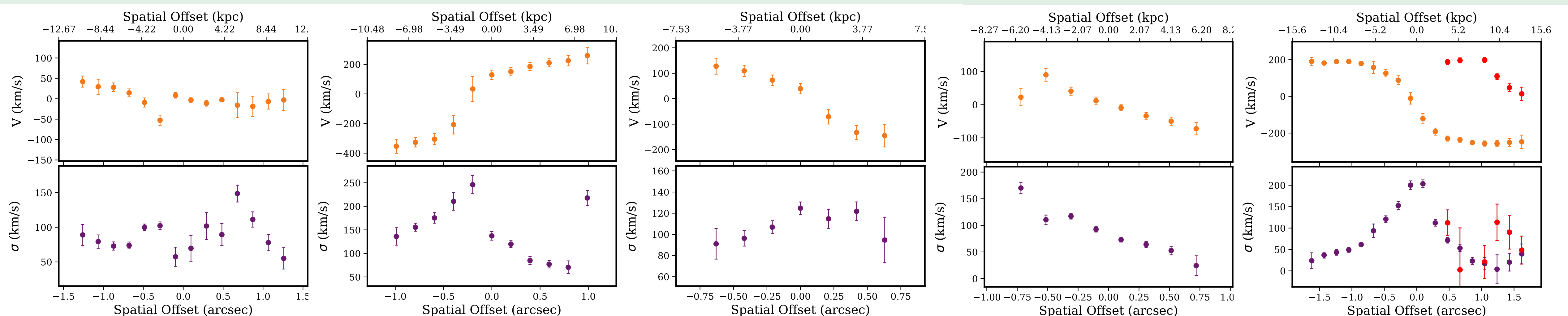
DSFG 450.25

DSFG 450.27

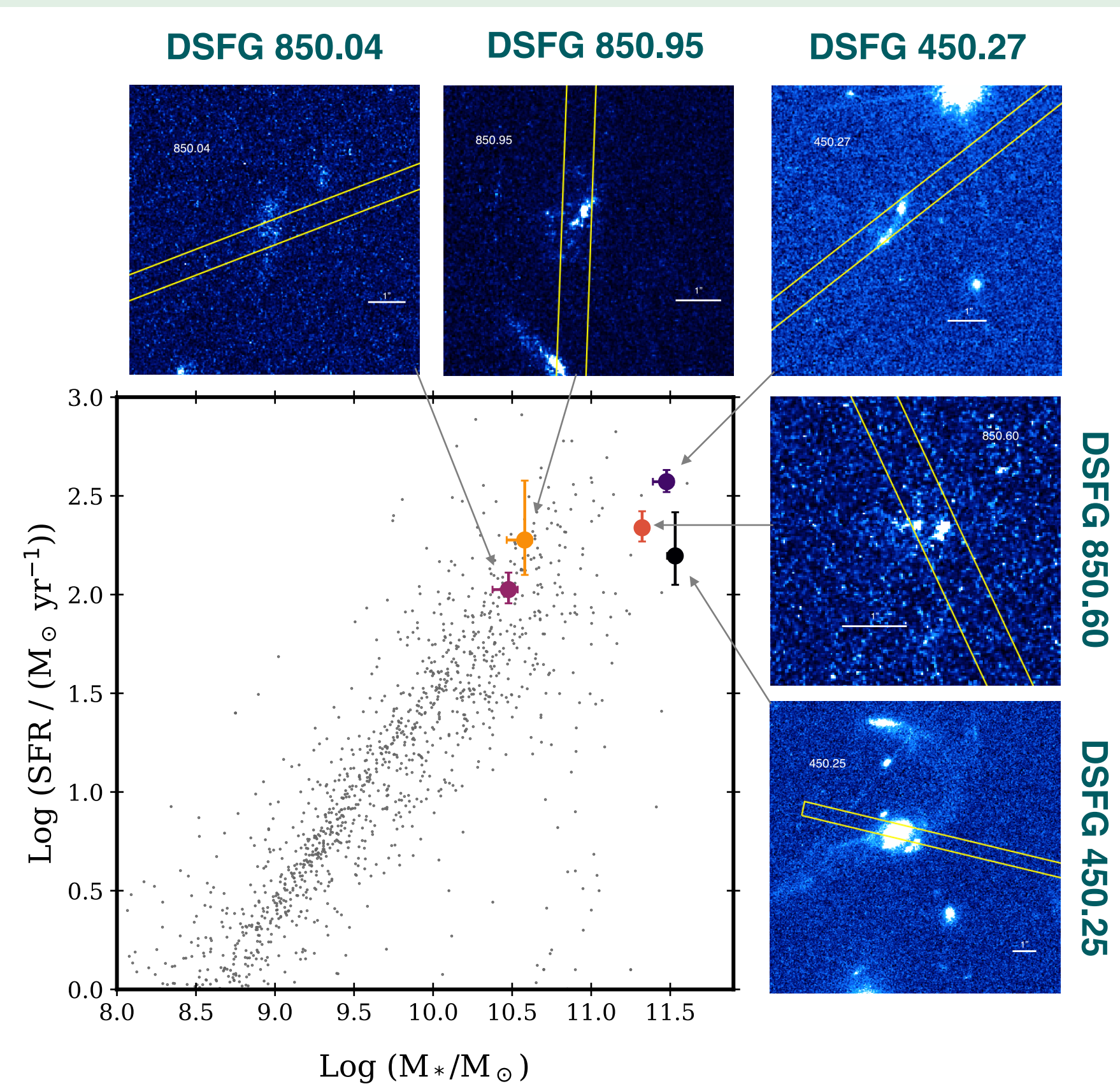
DSFG 850.04

DSFG 850.60

DSFG 850.95



## Main Sequence



Star formation rates and stellar masses are tight correlated at low redshift into a relation known as the main sequence of galaxies<sup>6</sup>. Merging systems have enhanced star formation and lie above the main sequence while systems that already underwent mergers and are now gas depleted lie below<sup>9</sup>. In our sample we find the opposite. **We find the three galaxies that are most likely to be merging systems, 450.25, 450.27, and 850.60, lie below the main sequence on the high stellar mass end.** This suggests the main sequence of galaxies may not be a useful discriminator of the mechanism of star formation in high redshift galaxies at the high-mass, high-SFR end.

Position-velocity and position-dispersion diagrams derived from our spectral fits. **850.95** shows clear signs of rotation, i.e. symmetric, smooth velocity and dispersion curves without discontinuities as well as centrally peaked dispersion<sup>6</sup>. The rotation curve flattens around 200 km/s, matching the peak dispersion velocity, which is typical of high- $z$  disk galaxies<sup>7</sup>. The red points on the righthand side represent a second object along the line of sight that is dispersion dominated rather than rotationally supported. **450.25** is undergoing a major merger. It exhibits discontinuities in velocity and dispersion and Hubble ACS imaging (see main sequence plot to the left) displays tidal tails. **450.27** has the largest range of radial velocities in our sample ( $\sim 600$  km/s). It also has a large discontinuity in velocity and dispersion. This suggests the two knots seen in Hubble ACS imaging to the left are likely to be two nuclei about to coalesce. **850.60** displays a roughly symmetric velocity curve but is without a centrally peaked dispersion, suggesting it is not rotationally supported. **850.04** has roughly symmetric velocity and dispersion curves. Hubble ACS imaging (see main sequence plot to the left) shows either an irregular morphology or is a clumpy, near edge-on disk. Because of (or despite) this ambiguity we estimate its dynamical mass (see table above).

Website:  
[www.patrickdrew.space](http://www.patrickdrew.space)



1) da Cunha, E., Charlot, S., & Elbaz, D. 2008, MNRAS, 388, 1595  
2) da Cunha, E., Walter, F., Smail, I. R., et al. 2015, ApJ, 806, 110  
3) Peng C. Y., Ho L. C., Impey C. D., Rix H., 2002, Astronomical J., 124, 266  
4) Peng C. Y., Ho L. C., Impey C. D., Rix H.-W. 2010, AJ, 139, 2097  
5) Chapman, S. C., Blain, A. W., Smail, I., & Ivison, R. J. 2005, ApJ, 622, 772

6) Genzel, R., Newman, S., Jones, T., et al. 2011, ApJ, 733, 101  
7) Glazebrook, K. 2013, PASA, 30, e056  
8) Noeske, K. G., Weiner, B. J., Faber, S. M., et al. 2007, ApJ, 660, L43  
9) Rodighiero, G., Daddi, E., Baronchelli, I., et al. 2011, ApJ, 739, L40  
This work is supported by a NASA Keck PI data Award, NSF grant PHY-1066293, and the University of Texas at Austin College of Natural Sciences.